J|A|C|S ARTICLES

Published on Web 04/01/2009

Mössbauer and DFT Study of the Ferromagnetically Coupled Diiron(IV) Precursor to a Complex with an $Fe^{IV}_2O_2$ Diamond Core

Marlène Martinho,[†] Genqiang Xue,[‡] Adam T. Fiedler,[‡] Lawrence Que, Jr.,*[,‡] Emile L. Bominaar,*[,†] and Eckard Münck*[,†]

Department of Chemistry, Carnegie Mellon University, Pittsburgh, Pennsylvania 15213, and Department of Chemistry and Center for Metals in Biocatalysis, University of Minnesota, 207 Pleasant Street SE, Minneapolis, Minnesota 55455

Received December 23, 2008; E-mail: larryque@umn.edu; eb7g@andrew.cmu.edu; emunck@cmu.edu

Abstract: Recently, we reported the reaction of the (μ-oxo)diiron(III) complex **1** ($[Fe^{III}_2(\mu\text{-}O)(\mu\text{-}O_2H_3)(L)_2]^{3+}$, L = tris(3,5-dimethyl-4-methoxypyridyl-2-methyl)amine) with 1 equiv of H_2O_2 to yield a diiron(IV) intermediate, **2** (Xue, G.; Fiedler, A. T.; Martinho, M.; Münck, E.; Que, L., Jr. *Proc. Natl. Acad. Sci. U.S.A.* **2008**, *105,* 20615−20). Upon treatment with $HClO_4$, complex **2** converted to a species with an $Fe^{IV}_2(\mu\text{-}O)_2$ diamond core that serves as the only synthetic model to date for the diiron(IV) core proposed for intermediate **Q** of soluble methane monooxygenase. Here we report detailed Mössbauer and density functional theory (DFT) studies of **2**. The Mössbauer studies reveal that **2** has distinct Fe^{IV} sites, **a** and **b**. Studies in applied magnetic fields show that the spins of sites **a** and **b** ($S_a = S_b = 1$) are ferromagnetically coupled to yield a ground multiplet with $S = 2$. Analysis of the applied field spectra of the exchange-coupled system yields for site **b** a set of parameters that matches those obtained for the mononuclear $[LFe^{IV}(O)(NCMe)]^{2+}$ complex, showing that site **b** (labeled Fe_O) has a terminal oxo group. Using the zero-field splitting parameters of $[LFe^{IV}(O)(NCMe)]^{2+}$ for our analysis of **2**, we obtained parameters for site **a** that closely resemble those reported for the nonoxo Fe^{IV} complex $[(\beta\text{-BPMCN})Fe^{IV}(OH)(OO^tBu)]^{2+}$, suggesting that **a** (labeled Fe_{OH}) coordinates a hydroxo group. A DFT optimization performed on **2** yielded an Fe−Fe distance of 3.39 Å and an Fe−(μ-O)−Fe angle of 131°, in good agreement with the results of our previous EXAFS study. The DFT calculations reproduce the Mössbauer parameters (**A**-tensors, electric field gradient, and isomer shift) of **2** quite well, including the observation that the largest components of the electric field gradients of Fe_O and Fe_{OH} are perpendicular. The ferromagnetic behavior of **2** seems puzzling given that the Fe−(μ-O)−Fe angle is large but can be explained by noting that the orbital structures of Fe_O and Fe_{OH} are such that the unpaired electrons at the two sites delocalize into orthogonal orbitals at the bridging oxygen, rationalizing the ferromagnetic behavior of **2**. Thus, inequivalent coordinations at Fe_O and Fe_{OH} define magnetic orbitals favorable for ferromagnetic ineractions.

Introduction

The conversion of methane to methanol in biological systems is carried out by methane monooxygenase (MMO).[1] The soluble form of this enzyme, sMMO, contains a nonheme diiron center in its active site that has been characterized thoroughly by kinetic, crystallographic, and spectroscopic methods.[2−5] The enzyme reacts with molecular oxygen to generate a series of intermediates; two that have attracted the most interest are a (μ-peroxo)diiron(III) species called **P** (or H_{peroxo})[6−8] and a diiron(IV) species called **Q**.[6,7,9] On the basis of EXAFS studies, it has been proposed that **Q** has an $Fe^{IV}_2(\mu\text{-}O)_2$ diamond core.[10] Kinetic studies show that **P** converts to **Q** in a proton-dependent core isomerization step.[11] Related to this conversion is the generation of the catalytically essential intermediate **X** of class 1 ribonucleotide reductases, which is formed in the reaction of O_2 with the diiron(II) center found in the R2 component of this enzyme. In this case, a (μ-peroxo)diiron(III) species also forms but subsequently undergoes one-electron reduction to generate the Fe^{III}−O−Fe^{IV} center in **X**.[12,13]

[†] Carnegie Mellon University.
[‡] University of Minnesota.

(1) Dalton, H. *Adv. Appl. Microbiol.* **1980**, *26*, 71–87.
(2) Wallar, B. J.; Lipscomb, J. D. *Chem. Rev.* **1996**, *96*, 2625–2657.
(3) Solomon, E. I.; Brunold, T. C.; Davis, M. I.; Kemsley, J. N.; Lee, S.-K.; Lehnert, N.; Neese, F.; Skulan, A. J.; Yang, Y.-S.; Zhou, J. *Chem. Rev.* **2000**, *100*, 235–350.
(4) Merkx, M.; Kopp, D. A.; Sazinsky, M. H.; Blazyk, J. L.; Muller, J.; Lippard, S. J. *Angew. Chem., Int. Ed.* **2001**, *40*, 2782–2807.
(5) Baik, M. H.; Newcomb, M.; Friesner, R. A.; Lippard, S. J. *Chem. Rev.* **2003**, *103*, 2385–2419.
(6) Lee, S. K.; Nesheim, J. C.; Lipscomb, J. D. *J. Biol. Chem.* **1993**, *268*, 21569–21577.
(7) Liu, K. E.; Valentine, A. M.; Wang, D.; Huynh, B. H.; Edmondson, D. E.; Salifoglou, A.; Lippard, S. J. *J. Am. Chem. Soc.* **1995**, *117*, 10174–10175.
(8) Valentine, A. M.; Stahl, S. S.; Lippard, S. J. *J. Am. Chem. Soc.* **1999**, *121*, 3876–3887.
(9) Lee, S. K.; Fox, B. G.; Froland, W. A.; Lipscomb, J. D.; Münck, E. *J. Am. Chem. Soc.* **1993**, *115*, 6450–6451.
(10) Shu, L.; Nesheim, J. C.; Kauffmann, K.; Münck, E.; Lipscomb, J. D.; Que, L., Jr. *Science* **1997**, *275*, 515–518.
(11) Lee, S. K.; Lipscomb, J. D. *Biochemistry* **1999**, *38*, 4423–4432.

10.1021/ja8098917 CCC: $40.75

Scheme 1. Reaction of **1** with H_2O_2 To Form **2**, **3**, and **4**

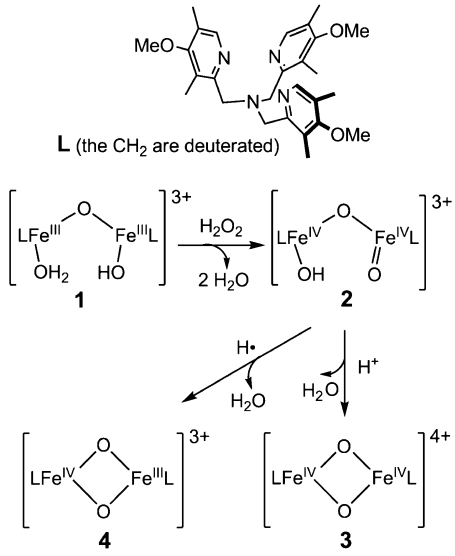

Biomimetic complexes have been useful in providing fundamental structure−spectroscopy correlations for interpreting the properties of enzyme intermediates. While there are now a number of synthetic oxoiron(IV) complexes that serve as models for oxoiron(IV) intermediates of nonheme monoiron enzymes,[14,15] there is only one synthetic complex characterized to have the $Fe^{IV}_2(\mu\text{-}O)_2$ diamond core motif proposed for sMMO intermediate **Q**.[16] In this initial effort, the synthetic complex $[Fe^{IV}_2(\mu\text{-}O)_2(L)_2]^{4+}$ (**3**, L = tris(3,5-dimethyl-4-methoxylpyridyl-2-methyl)amine) was obtained by one-electron oxidation of its $Fe^{III}Fe^{IV}$ precursor (Scheme 1; we label the compounds as in ref 17). More recently, however, we have discovered that **3** can also be generated from the reaction of a (μ-oxo)diiron(III) complex and H_2O_2, a transformation that may shed light on steps in the enzymatic **P** to **Q** conversion.[17] Treatment of $[Fe^{III}_2(\mu\text{-}O)(OH)(H_2O)(L)_2](ClO_4)_3$, **1** (the methylene groups of L were deuterated), with 1 equiv of H_2O_2 affords intermediate **2** in 60−80% yield. Addition of 1 equiv of $HClO_4$ instantly converts **2** into **3**, forming the $[Fe^{IV}_2(\mu\text{-}O)_2]$ diamond core. In the presence of H-atom donors, intermediate **2** converts to the well-characterized[18] green $[Fe^{IV}Fe^{III}(\mu\text{-}O)_2(L)_2]^{3+}$ intermediate, **4**. The presence of **4** is easily recognized by its characteristic $S = {}^3/_2$ EPR signal and Mössbauer quadrupole doublet with $\Delta E_Q = 0.44$ mm/s and isomer shift, $\delta = 0.11$ mm/s (a doublet is observed for $T > 70$ K).

Complex **2** is thus an interesting precursor to complexes with $Fe_2(\mu\text{-}O)_2$ cores. Electrospray ionization mass spectrometry (ESI-MS) of **2** showed an ion cluster with a mass and isotope distribution pattern consistent with the formulation $\{[(Fe_2O_3(L)_2H)](OTf)_2\}^+$, and ^{18}O-labeling studies demonstrated that one oxygen atom derives from the diiron(III) precursor while the other two originate from H_2O_2.[17] EXAFS studies revealed the presence of a 1.66-Å Fe−O bond associated with an Fe=O unit and an Fe−Fe distance of 3.32 Å.[17] Mössbauer studies of **2** revealed a diiron(IV) center with inequivalent iron(IV) sites, one of which with Mössbauer parameters, reported below, strikingly similar to those of the mononuclear complex $[LFe^{IV}(O)(NCMe)]^{2+}$. These data lead us to propose that **2** is a complex with a structure as depicted in Figure 1 having an HO−Fe^{IV}−O−Fe^{IV}=O core.

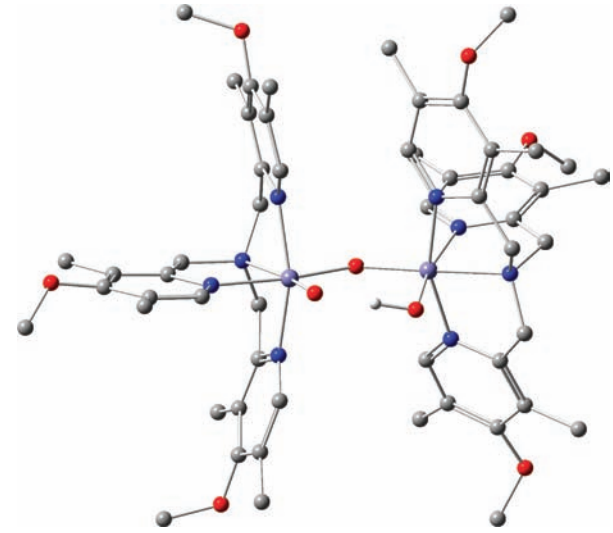

Figure 1. DFT-optimized structure of **2** (ADF optimization, method 1). Hydrogen atoms have been omitted for clarity, except for the one of the hydroxo ligand on the Fe_{OH} site.

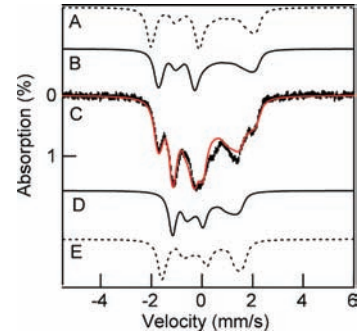

Figure 2. Mössbauer spectrum of **2** recorded at 80 K in a parallel applied field of 8.0 T (hash marks in C). The solid line is a spectral simulation generated from eq 1 in the strong coupling limit, using the parameters quoted in Table 1, with slight modifications as discussed later in this work. The dashed lines A and E are simulations assuming diamagnetism for paramagnetic sites **a** and **b**, respectively. The solid lines B and D are simulations for sites **a** and **b**, respectively.

In ref 17 we touched only briefly on the Mössbauer properties of **2**, showing only a 4.2 K spectrum recorded in zero applied magnetic field. Here we report a detailed Mössbauer study of **2**, together with a spin Hamiltonian analysis, that reveals **2** to be a ferromagnetically coupled diiron(IV) complex, containing one site with a terminal oxo ligand. We also report density functional theory (DFT) studies that give insight into the structure of **2** and rationalize the observed ferromagnetic coupling.

Materials and Methods

Complex **2** in MeCN was prepared by a previously described procedure.[17] The Mössbauer analysis was performed on a sample

(12) Wei, P. P.; Skulan, A. J.; Mitic, N.; Yang, Y. S.; Saleh, L.; Bollinger, J. M.; Solomon, E. I. *J. Am. Chem. Soc.* **2004**, *126*, 3777–3788.
(13) Yun, D.; Garcia-Serres, R.; Chicalese, B. M.; An, Y. H.; Huynh, B. H.; Bollinger, J. M. *Biochemistry* **2007**, *46*, 1925–1932.
(14) Que, L., Jr. *Acc. Chem. Res.* **2007**, *40*, 493–500.
(15) Shan, X.; Que, L., Jr. *J. Inorg. Biochem.* **2006**, *100*, 421–433.
(16) Xue, G.; Wang, D.; De Hont, R.; Fiedler, A. T.; Shan, X.; Münck, E.; Que, L., Jr. *Proc. Natl. Acad. Sci. U. S. A.* **2007**, *104*, 20713–20718.
(17) Xue, G.; Fiedler, A. T.; Martinho, M.; Münck, E.; Que, L., Jr. *Proc. Natl. Acad. Sci. U. S. A.* **2008**, *105*, 20615–20620.
(18) Dong, Y.; Fujii, H.; Hendrich, M. P.; Leising, R. A.; Pan, G.; Randall, C. R.; Wilkinson, E. C.; Zang, Y.; Que, L., Jr.; Fox, B. G.; Kauffmann, K.; Münck, E. *J. Am. Chem. Soc.* **1995**, *117*, 2778–2792.

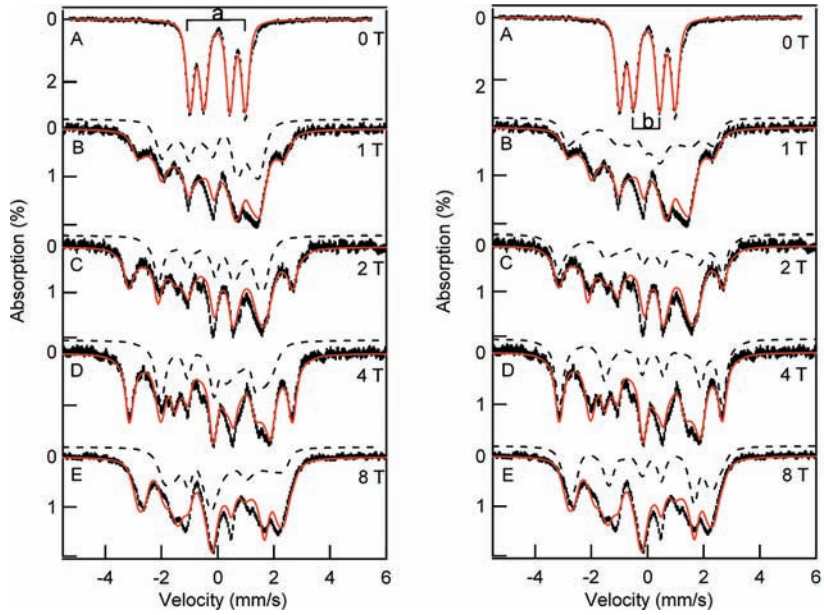

Figure 3. 4.2 K Mössbauer spectra of **2** in a 1:1 mixture of acetonitrile/butyronitrile recorded in applied magnetic fields as indicated. The solid lines represent spectral simulations based on eq 1 using the parameters listed in rows 2 and 3 of Table 1. Left panel: The dashed lines are simulations for site **a**. Right panel: Same data and solid lines as in left panel, with the dashed lines representing simulations for site **b**. For $B > 2$ T the magnetic splitting of **b** decreases as a function of increasing field, showing that $B_{int}(\mathbf{b}) < 0$.

Table 1. Zero-Field Splittings and Hyperfine Parameters of **2** and Two Relevant Mononuclear Complexes[a]

	D (cm^{-1})	E/D	$A_x/g_n\beta_n$ (T)	$A_y/g_n\beta_n$ (T)	$A_z/g_n\beta_n$ (T)	A_{iso} (T)	ΔE_Q (mm/s)	η	δ (mm/s)
$[LFe^{IV}(O)(NCMe)]^{2+}$	27	0	−23.0	−23.0	−4.0	−16.7	+0.95	0.8[b]	0.01
site **b** (Fe_O)	27[c]	0	−23.0	−22.7	−5.0	−16.9	+0.92	0[b]	−0.03
site **a** (Fe_{OH})	−1.35	−8.75[d]	+0.4	−11.0	−20.0	−10.2	−1.96	−3[e]	0.0
site **a** (proper frame)	17.7[f]	0.28	−20.0	−11.0	+0.4	−10.2	+1.96	0	0.0
$[(\beta\text{-BPMCN})Fe^{IV}(OH)(OO\mathit{t}Bu)]^{2+}$[g]	16	0.20	−15.5	−21.0	−6.0	−14.1	+1.76	0.6	0.1

[a] Rows 2 and 3 present the parameters of **2** expressed in $\{x, y, z\}$. Row 4 lists the parameters of site **a** in the proper coordinate system, $\{x^p, y^p, z^p\}$, of its ZFS tensor. For the simulations we used $J = -50$ cm^{-1}. The parameters are quoted in the uncoupled representation of eq 1. Rows 1 and 5 list the Mössbauer parameters of two mononuclear Fe^{IV} complexes. [b] For the complexes studied here it is difficult to determine the asymmetry parameter η with precision. For **b** we estimate $0 < \eta < 0.4$, and $0.6 < \eta < 1$ for $[LFe^{IV}(O)(NCMe)]^{2+}$. [c] For site **b** we have adopted the D-value of $[LFe^{IV}(O)(NCMe)]^{2+}$. [d] $E/D = -8.75$ implies that largest component of **D**-tensor is along x. [e] $\eta = -3$ implies that the EFG tensor is axial around x. [f] The ZFS parameter D_a (= 17.7 cm^{-1} quoted in its proper frame) is quite sensitive to the choice of J, and is thus rather soft. [g] Parameters from Jensen et al.[29]

prepared in 1:1 MeCN−PrCN mixture. To prepare this sample, **1** dissolved in MeCN was treated with 0.8 equiv of H_2O_2 in MeCN at −40 °C to generate **2**; an equal volume of PrCN (precooled to −40 °C) was then added prior to freezing the solution. We also prepared a sample of **2** by treating **1** with 1 equiv of D_2O_2 in MeCN at −40 °C. Mössbauer spectra were collected with constant acceleration spectrometers, using two cryostats that allowed studies at 4.2 K in applied fields up to 8.0 T. Isomer shifts are quoted relative to Fe metal at 298 K. Spectra were analyzed with the WMOSS software package (WEB Research Co., Edina, MN). Density functional theory (DFT) calculations were performed for complex **2** by using the Amsterdam Density Functional (ADF) 2008.01 software package[19−21] on a cluster of 10 processors (Ace computers) using ADF basis set IV (triple-ζ with single polarization on the ligand atoms), an integration constant of 4.0, and the Vosko−Wilk−Nusair local density approximation[22] with the non-local gradient corrections of Becke[23] and Perdew[24] (BPVWN) (method 1) and by using Becke's three parameter hybrid (B3LYP) functional and basis set 6−311G provided by Gaussian 03 software package[25] on a cluster of 8 processors[26] (method 2). One calculation was performed using the same approach as that of method 2 but using the PBEVWN functional instead of the B3LYP (method 3). For details of the DFT study, see the Supporting Information.

Mössbauer Analysis

We have studied with Mössbauer spectroscopy samples of **2** (14 preparations) treated with 0.2, 0.4, 0.6, 0.8, 1.0, 1.2, 1.5, and 2.0 equiv of H_2O_2 in acetonitrile and 1:1 acetonitrile/butyronitrile mixtures, with the goal of studying the formation of **2** and maximizing the content of **2** in a sample for comprehensive studies in strong applied magnetic fields. For a detailed study we have selected a sample obtained by adding 0.8 equiv of H_2O_2 to the diferric starting material, **1**, in a 1:1 acetonitrile/butyronitrile mixture at −40 °C. Figures 2, 3, and S5 show Mössbauer spectra recorded for this sample.

Our samples generally contained diferric contaminants and a small amount of the green $S = {}^3/_2$ $Fe^{III}Fe^{IV}$ intermediate **4**;

(19) te Velde, G.; Baerends, E. J. *J. Comput. Phys.* **1992**, *99*, 84–98.
(20) Guerra, C. F.; Snijders, J. G.; Te Velde, G.; Baerends, E. J. *Theor. Chem. Acc.* **1998**, *99*, 391–403.
(21) *ADF 2008.01*; SCM, Theoretical Chemistry, Vrije Universiteit: Amsterdam, The Netherlands, http://www.scm.com.
(22) Vosko, S. H.; Wilk, L.; Nusair, M. *Can. J. Phys.* **1980**, *58*, 1200–1211.
(23) Becke, A. D. *J. Chem. Phys.* **1986**, *84*, 4524–4529.
(24) Perdew, J. P. *Phys. Rev. B* **1986**, *33*, 8822–8824.
(25) Frisch, M. J.; et al. *Gaussian 03,* revision E.01; 2004.
(26) Catlett, C. *TeraGrid: Analysis of Organization, System Architecture, and Middleware Enabling New Types of Applications, HPC and Grids in Action*; Grandinetti, L., Ed.; IOS Press: Amsterdam, 2007.

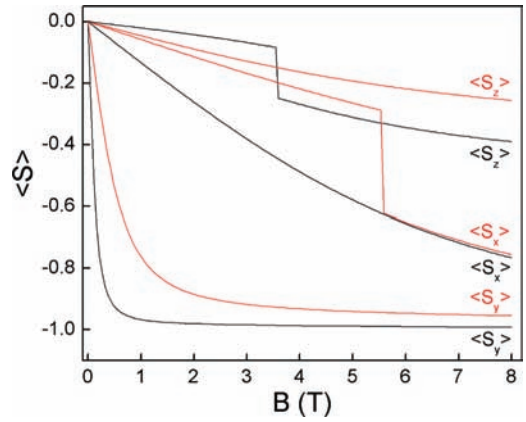

Figure 4. Expectation values of the components of the electronic spin for the *lowest* spin level of **2**, with the external field B applied along x, y, and z. Black: Curves generated for the zero-field splitting parameters of Table 1 using $J = -1000$ cm^{-1}, the strong coupling limit. Except for a scaling factor 2, the same curves are obtained in the coupled representation using $D = 4.29$ cm^{-1}, $E/D = 0.44$, and $g_e = 2$ in eq 2. In the strong coupling limit $\langle S_i\rangle_{\mathbf{a}} = \langle S_i\rangle_{\mathbf{b}}$. Red: Same zero-field splitting parameters as for the black curves but $J = -50$ cm^{-1}. The breaks in the curves are due to level crossings.

typically, around 5% of the Mössbauer absorption could not be accounted for (reflecting probably residuals of imperfect subtractions). The diferric contaminants, identified by the observation of diamagnetic components with isomer shift $\delta \approx 0.45$ mm/s, may comprise three different species in variable proportions, namely (i) nonreacted starting complex **1**, (ii) an $[Fe_2^{III}(O)(H_2O)_2(L)_2]^{4+}$ contaminant in the starting material (which does not afford **2** upon addition of peroxide), and (iii) a diferric decay product. Figure S5A shows a 4.2 K zero-field Mössbauer spectrum of the sample described below; after subtraction of the contaminants, described in Supporting Information, we obtained the spectrum of **2** shown in Figure 3A. The spectrum exhibits two quadrupole doublets assigned to intermediate **2**.

The prepared Mössbauer spectra of Figures 2 and 3 were obtained by subtracting the contributions of **1** (35%) and **4** (5%) from the raw data. The zero-field spectrum of Figure 3A consists of two nested quadrupole doublets, each representing ≈30% of the Fe in the sample. Doublet **a** (called site **a** in this section) has $\Delta E_Q(\mathbf{a}) = 1.96$ mm/s and $\delta(\mathbf{a}) = 0.00$ mm/s while doublet **b** (site **b**) exhibits $\Delta E_Q(\mathbf{b}) = 0.92$ mm/s and $\delta(\mathrm{b}) = -0.03$ mm/s. The isomer shifts of **a** and **b** are characteristic of Fe^{IV} TPA complexes (TPA = tris(pyridyl-2-methyl)amine),[15] an assignment supported by the observation that both are transformed upon protonation into the red diiron(IV) intermediate **3** with $\delta = -0.05$ mm/s and $\Delta E_Q = 2.01$ mm/s. Doublets **a** and **b** always appeared in a 1:1 ratio when the diferric complex **1** was titrated with H_2O_2. (We found that the amount of **3** obtained by protonation correlates very well with the amount of **2** determined by the Mössbauer analysis.)

Both **a** and **b** exhibit quadrupole doublets at 4.2 K, showing that they belong to a complex with integer electron spin. In applied magnetic fields, B, the spectra of **a** and **b** exhibit paramagnetic hyperfine structure, implying that the ground-state of **2** has electronic spin $S > 0$. The whole body of our Mössbauer analysis suggests that **a** and **b** are subsites of a dinuclear complex. Given that **2** originates from dimer **1** and transforms, respectively, into dimers **3** and **4** upon protonation and hydrogen atom transfer,[17] it was expected from the outset that **2** is a dimer (mass spectrometric data[17] led to the same conclusion). The spectra recorded in applied fields are exceedingly complex, and they depend on numerous unknowns. However, the salient features of the solution can be recognized, albeit with some effort, by inspection of the data.

We first consider the 8.0 T spectrum of Figure 2C recorded at 80 K, a temperature at which the electronic spin of **2** is in the fast relaxation limit. A spectral simulation (Figure 2A, dashed) assuming diamagnetism for site **a** yields for the low-energy feature (see comment in ref 27) a splitting substantially larger than observed experimentally, indicating that the ^{57}Fe nucleus of site **a** experiences an effective field, $B_{\mathrm{eff}} = B + B_{\mathrm{int}}$, that is ca. 2−3 T smaller than the applied field. Indeed, the simulation with $B_{\mathrm{int}} = -2.5$ T (along x and y), shown in Figure 2B, fits the data quite well. Corresponding simulations, shown in Figure 2D,E (dashed), reveal that site **b** has a negative B_{int} as well. A negative B_{int} for both sites indicates that the local spins $S_{\mathbf{a}}$ and $S_{\mathbf{b}}$ are parallel and that **2**, therefore, is a *ferromagnetically* coupled diiron(IV) complex.[27] All Fe^{IV}−TPA complexes studied to date have $S = 1$, and thus we can reasonably assume that the local sites **a** and **b** have $S_{\mathbf{a}} = S_{\mathbf{b}} = 1$.

We have analyzed the applied field spectra of **2** in the framework of the spin Hamiltonian

$$\hat{H} = J\hat{\mathbf{S}}_{\mathbf{a}}\cdot\hat{\mathbf{S}}_{\mathbf{b}} + \sum_{i=\mathbf{a},\mathbf{b}} \{D_i(\hat{S}_{iz}^2 - 2) + E_i(\hat{S}_{ix}^2 - \hat{S}_{iy}^2) + g_e\beta\mathbf{B}\cdot\hat{\mathbf{S}}_i + \hat{\mathbf{S}}_i\cdot\mathbf{A}_i\cdot\hat{\mathbf{I}}_i - g_n\beta_n\mathbf{B}\cdot\hat{\mathbf{I}}_i + \hat{H}_Q(i)\} \quad (1)$$

where J is the isotropic exchange coupling constant ($J < 0$). $D_{\mathbf{a}}$, $D_{\mathbf{b}}$ and $E_{\mathbf{a}}$, $E_{\mathbf{b}}$ are the axial and rhombic (local) zero-field splitting (ZFS) parameters of the $S_{\mathbf{a}} = 1$ and $S_{\mathbf{b}} = 1$ multiplets. The remaining terms describe the electronic Zeeman, magnetic hyperfine, nuclear Zeeman, and electric quadrupole interactions. $S = 1$ Fe^{IV} complexes generally have $g \approx 2$, and therefore we have fixed the g-values at $g_e = 2$. In the limit of strong ferromagnetic coupling, $|J| \gg |D_i|$, the ground-state of **2** is a multiplet with $S = 2$ for which the electronic terms of eq 1 can be rewritten as

$$\hat{H}_e = D(\hat{S}_z^2 - 2) + E(\hat{S}_x^2 - \hat{S}_y^2) + 2\beta\mathbf{B}\cdot\hat{\mathbf{S}} \quad (2)$$

In eq 2 the ZFS tensor of the $S = 2$ multiplet is given by[28]

$$\mathbf{D} = \frac{\mathbf{D}_{\mathbf{a}} + \mathbf{D}_{\mathbf{b}}}{6} \quad (3)$$

In the strong coupling limit the nuclear part of eq 1 can be written as ($S = 2$)

$$\hat{H}_{\mathrm{nucl}} = \sum_{i=\mathbf{a},\mathbf{b}} \left\{\frac{1}{2}\hat{\mathbf{S}}\cdot\mathbf{A}_i\cdot\hat{\mathbf{I}}_i - g_n\beta_n\mathbf{B}\cdot\hat{\mathbf{I}}_i + \hat{H}_Q(i)\right\} \quad (4)$$

The factor $^1/_2$ is a spin projection factor[28] that has to be included when the local spin operators $\hat{S}_a$ and $\hat{S}_b$ are replaced by the cluster spin operator $\hat{S}$. In order to discover the nature of the solution it will be useful to discuss the problem first in the strong coupling limit and use eqs 2 and 4, $\hat{H} = \hat{H}_e + \hat{H}_{\mathrm{nucl}}$. Throughout this section we will take the principal axis system of **D**, $\{x, y, z\}$, as the frame of reference. In order to keep the number of unknowns manageable we assume that all tensors are diagonal in $\{x, y, z\}$, but allow 90° rotations around a principal axis.

$\hat{H}_Q$ of eqs 1 and 4 can be written in its commonly used principal axis form (dropping the site index i) as

$$\hat{H}_Q = \left(\frac{eQV_{zz}}{12}\right)\left(3\hat{I}_z^2 - \frac{15}{4} + \eta(\hat{I}_x^2 - \hat{I}_y^2)\right) \quad (5)$$

where $\eta = (V_{xx} - V_{yy})/V_{zz}$ is the asymmetry parameter of the electric field gradient (EFG) tensor. For $\eta = 0$, -3, and $+3$ the EFG is axial around z, x, and y, respectively.

For reasonably small values of D (say, $D < 10$ cm^{-1}) the 80 K, 8.0 T spectrum of Figure 2 is (essentially) independent of D, and the thermally averaged expectation values of the site spins, $\langle S_a\rangle_{th} = \langle S_b\rangle_{th} = (^1/_2)\langle S\rangle_{th}$, are small and follow the Curie law above 50 K. Under these conditions the two sites can be treated independently (**D** correlates the spatial directions of the two sites at 4.2 K), and we can obtain valuable information about the EFG- and **A**-tensors. We temporarily use the independent frames $\{X',Y',Z'\}$ for site **a** and $\{X'',Y'',Z''\}$ for site **b**: we will shortly relate these frames with $\{x, y, z\}$ and the molecular frame of **2**.

Spectral simulations suggested the following parameters: for site **a**, $\Delta E_Q = +1.96$ mm/s, $\eta \approx 0$, $A_{X'}/g_n\beta_n \approx A_{Y'}/g_n\beta_n \approx -(15-16)$ T, and $A_{Z'}/g_n\beta_n \approx +0.4$ T; for site **b**, $\Delta E_Q = +0.92$ mm/s, $\eta \approx 0$, $A_{X''}/g_n\beta_n \approx A_{Y''}/g_n\beta_n = -23$ T, and $A_{Z''}/g_n\beta_n \approx -5$ T. Importantly, the 80 K/8.0 T spectrum tolerates $A_{X'} \neq A_{Y'}$ as long as their average, roughly, corresponds to the above quoted axial range. The possibility that $A_{X'} \neq A_{Y'}$ for site **a** enabled us to find a solution that fits both the 80 and 4.2 K spectra.

At 4.2 K, the electronic spin, $S = 2$, of **2** is in the slow relaxation limit on the time scale of Mössbauer spectroscopy ($\approx 10^{-7}$ s). The spectra show that the magnetic hyperfine splittings of both iron sites increase with increasing applied field, reaching their saturation values near $B = 2$ T. (In order to "see" that, one must have recognized the associations of doublets **a** and **b** with the high-field features of the spectra; the authors labored for many hours on this problem.) Such saturation behavior is approximately described by eq 2 for $D \approx 4$ cm^{-1} and $E/D \approx 0.4$ (Figure 4, black curves). Although the 4.2 K spectra are quite complex, we can understand their principal features from the following considerations. The magnitudes of the (negative) expectation values of the electronic ground level along y, x, and z are ordered such that $|\langle S_y\rangle| \geq |\langle S_x\rangle| > |\langle S_z\rangle|$ (see Figure 4). For acceptable simulations for site **b** we must align $\{X'', Y'', Z''\}$ with $\{x, y, z\}$ such that $Z'' = z$. In order to produce the correct 4.2 K magnetization for site **a**, i.e., the correct $\langle S_y\rangle$, we must have, in $\{x, y, z\}$, $A_y/g_n\beta_n \approx -11$ T, which would yield $A_x/g_n\beta_n \approx -(20)$ T (if $X' \equiv x$), as the two components must average to about $-(15-16)$ T. However, we need a solution for which the largest **A**-tensor component is multiplied by a small expectation value of S_a, namely $\langle S_{z,a}\rangle$; without this association the calculated magnetic splittings for site **a** would considerably exceed the experimentally observed splittings at 4.2 K. The suggested associations are made by having the largest component of the EFG along x (which can be accomplished by replacing $\eta' = 0$ with $\eta = -3$ and working in $\{x, y, z\}$) and associating $A_{X'}$ with A_z. These associations imply that the largest components of the EFGs of sites **a** and **b** are perpendicular to each other.

In the course of our studies we noticed that the hyperfine parameters obtained for site **b** are very close to those observed for $S = 1$ Fe^{IV}=O complexes, an observation that prompted us to synthesize and study the Fe^{IV}−oxo complex $[LFe^{IV}(O)(N\text{-}CMe)]^{2+}$ with the same TPA-related ligand; Mössbauer data, analysis, and optimized DFT structure for this complex are presented in Supporting Information. Comparison of the parameters of the mononuclear complex in Table 1 with those obtained for site **b** forcefully suggests that site **b** has a terminal oxo ligand. The analysis of the Mössbauer spectra of **2** required as many as 1000 spectral simulations, and throughout this effort we had little idea what structure gave rise to this ferromagnetically coupled diiron(IV) complex. Thus, finding a parameter set for site **b** that closely matched those of an Fe^{IV}=O complex, prior to obtaining the EXAFS and mass spectrometric evidence,[17] would suggest that the decomposition of the spectra is essentially reliable.

With the strong hint that **b** is an Fe^{IV} site with terminal oxo group we switched to the uncoupled representation of eq 1. Using the approximate values of D and E/D obtained in the strong exchange coupling limit (pure $S = 2$ ground multiplet) and inserting $D_b = 27$ cm^{-1} and $(E/D)_b = 0$ into eq 3, we obtained a reasonable approximation for D_a and $(E/D)_a$. We then performed a global search, keeping D_a, $(E/D)_a$, and the EFGs of both sites fixed. Lowering the magnitude of J from the strong exchange coupling limit decreases the spin expectation values by multiplet mixing by the D_a and D_b terms (Figure 4, red curves) and requires slightly larger A_y values for fitting the magnetization behavior [i.e., fitting $B_{int,a,b}$ vs B]. Our "best" solution set (listed in Table 1) was obtained for $J \approx -50$ cm^{-1}; this set has $D_a = -1.35$ cm^{-1} and $(E/D)_a = -8.75$ when quoted in $\{x, y, z\}$. By using quotation marks we remind the reader that the data of Figures 2 and 3 were obtained by subtracting 40% of the absorption attributable to contaminants from the raw data. It is likely that one can find solution sets of similar quality for any J value in the range -150 cm^{-1} $< J <$ -30 cm^{-1}. However, for $-J < 30$ cm^{-1} the magnetic splittings of sites **a** and **b** would saturate observably differently.

Rows 2 and 3 of Table 1 list the parameters of sites **a** and **b** in $\{x, y, z\}$. This frame is the "proper" coordinate system of the ZFS tensor of oxo site **b** (frames for which $0 \leq (E/D) \leq {}^1/_3$ or $0 \leq \eta \leq 1$ are often called "proper"). The proper coordinate frame of site **a**, $\{x^p, y^p, z^p\}$, has its z^p-axis along x. (The use of a proper frame for D_a facilitates comparison of the parameters of site **a** with published work.) Row 4 lists the parameters of site **a** in $\{x^p, y^p, z^p\}$; in this frame $D_a = +17.7$ cm^{-1} and $(E/D)_a = 0.28$. These values together with the large ΔE_Q of site **a** pointed our attention to a Mössbauer study of the mononuclear complex $[(\beta\text{-BPMCN})Fe^{IV}(OH)(OO^tBu)]^{2+}$.[29] Guided by the observation of an $\{[Fe_2O_3L_2H](OTf)_2\}^+$ cation by ESI-MS, we picture site **a** as an L−Fe^{IV} complex with a hydroxide ligand and linked by an oxo bridge to site **b**, and interestingly, the Mössbauer parameters of site **a** and the monomeric BPMCN complex (Table 1) are intriguingly similar (the proximal oxygen of the peroxo group representing the bridging oxygen of **2**).

We have made some observations we do not yet fully understand. In order to demonstrate ferromagnetic coupling for **2**, we have discussed, for developing the argument rather than out of necessity, the 80 K spectrum of Figure 2C in the limit of strong

(27) At 80 K, the internal field at site i can be written as $\mathbf{B}_{int,i} = -\langle \mathbf{S}_i\rangle_{th} \cdot \mathbf{A}_i/g_n\beta_n$, where $\langle \mathbf{S}_i\rangle_{th}$ is the thermally averaged spin of site i and $\mathbf{A}_i$ is the magnetic hyperfine tensor. The argument for parallel spin alignment draws on the observation that the major components of the **A**-tensors of Fe^{IV}−TPA complexes are negative, typically $A_x/g_n\beta_n \approx A_y/g_n\beta_n = -23$ T, $A_z/g_n\beta_n = -5$ T; see below. Because of the small A_z values the high energy features in Figure 2C (at +1.5 mm/s and +2.5 mm/s) exhibit very small internal fields.

(28) Bencini, A.; Gatteschi, D. *EPR of Exchange Coupled Systems*; Springer-Verlag: New York, 1990.

(29) Jensen, M. P.; Costas, M.; Ho, R. Y. N.; Kaizer, J.; Payeras, A. M. I.; Münck, E.; Que, L.; Rohde, J. U.; Stubna, A. *J. Am. Chem. Soc.* **2005**, *127*, 10512–10525.

exchange coupling ($B_{int,\mathbf{b}} < 0$ can be also inferred from inspection of the spectra of Figure 3, dashed lines). This allowed us to focus on the fact that B_{int} is negative for both sites of **2**. After many attempts to simulate the low temperature spectra, we arrived at a set for which the magnitude of J is comparable to $D_{\mathbf{a}}$ and $D_{\mathbf{b}}$. The parameter set of Table 1 describes all essential features of the 4.2 K spectra. However, for matching the simulations to the 80 K spectrum as shown in Figure 2 we had to increase A_x and A_y of site **b** by ca. 8%. We also increased A_z of site **a** from −20 to −28 T ($\langle S_z \rangle$ is small at 4.2 K, and thus the quoted value of $A_{z,\mathbf{a}}$ is soft). It is possible that our J-value and ZFS-tensors are not optimal to describe the temperature dependence of the thermally averaged expectation values of the electronic spin system. However, there may be other reasons for the requirement of using slightly different A-values at 80 K. Thus, as shown in Figure S6, the recoilless fraction (Debye−Waller factor) of site **a** drops precipitously above 80 K, indicating, perhaps, a structural change, possibly of dynamic nature (such as a rotation of the hydroxo ligand or proton hopping).[30]

Comparison with the DFT Calculations

In this section we examine the parameters of Table 1 and compare them with the results of a DFT study of **2**. To aid the reader in this discussion we will relabel site **a** as Fe_{OH} and site **b** as Fe_O. Using the procedures described in Supporting Information, we have performed a series of geometry optimizations of **2** using as the starting configuration the X-ray structure of $[Fe^{III}_2(O)(OH)(OH_2)(5\text{-}Me_3TPA)_2]^{3+}$ (5-Me_3-TPA = tris(5-methylpyridyl-2-methyl)amine), a complex closely related to **1**, in which the water and hydroxo ligands have been replaced by hydroxo and oxo groups, respectively.[18] The optimized structure of diiron(IV) complex **2**, using method 1, is shown in Figure 1. The calculated structure has an Fe−Fe distance of 3.39 Å (*3.32* Å), an Fe−oxo bond length of 1.67 Å (*1.66* Å), and an Fe−O−Fe angle of 130.8°, in good agreement with the metric data obtained from EXAFS[17] (listed in italics). In the DFT structure the proton of the hydroxo group of site Fe_{OH} is hydrogen bonded to the oxo group of site Fe_O.

The calculations reported here (see tables and text in Supporting Information) reveal significant differences in the structure of the $O_TFe_OO_BFe_{OH}OH$ core (T = terminal, B = bridge), depending on the functional/basis set combination used for the geometry optimization. The structural discrepancies may be rooted in differences between the functionals in their ability to assess the hydrogen bonding between OH and O_T (see Supporting Information). In particular, BPVWN/IV (method 1) used for the calculation of the structure in Figure 1 yields an approximately planar core, whereas B3LYP/6−311G (method 2) results in a nonplanar core unit. Since the 3d-electron-carrying t_{2g} orbitals of Fe_{OH} are engaged in π interactions with the lone-pair orbitals of OH and the bridging oxygen, O_B, the torsion angles of the core unit affect the composition of the t_{2g} orbitals (and their energies) and with it properties such as the EFG-tensor and the spin-dipolar part of the magnetic hyperfine tensor ($\mathbf{A}_{SD}$). Particularly affected are the orientations of the principal tensor axes through torsion of the terminal hydroxide at Fe_{OH}. The principal axes in the optimized structure obtained by method 2 are rotated more away from the Fe_{OH}−ligand bonds than in the optimized structure obtained by method 1, where the core exhibits less torsion.

For small torsions, as in the optimized structures obtained with method 1, the principal axes of the largest component of EFG and $\mathbf{A}_{SD}$ tensors at the Fe_{OH} site are nearly parallel and roughly align with the $N_{trans}-N_{trans}$ direction, whereas in the case of large torsions, as obtained with method 2, these axes deviate significantly from this direction. For the following qualitative discussions we adopt the solution of method 1, unless stated otherwise, for two reasons. First, the ADF program is more convenient for broken symmetry calculations to assess the exchange interactions, and second, the consistency of the description provided by method 1 with the Mössbauer analysis presented above is easier to judge than for method 2. This does not mean that the solution obtained with method 2 can be dismissed. We wish to stress that the principal axes of the EFG- and $\mathbf{A}_{SD}$-tensors of the Fe_O site, where the t_{2g} orbitals form strong π bonds with the p orbitals of the terminal oxo ligand, are insensitive to the methodological differences affecting the core structure.

The ^{57}Fe magnetic hyperfine tensor can, in general, be written as $\mathbf{A} = A_C + \mathbf{A}_{SD} + \mathbf{A}_L$. A_C is the isotropic Fermi contact term, $\mathbf{A}_{SD}$ describes the traceless spin-dipolar contribution, and $\mathbf{A}_L$ accounts for the orbital contribution. $\mathbf{A}_L$ can be decomposed into an isotropic (pseudocontact) part, A_{PC}, and a traceless anisotropic part, $\mathbf{A}_{L,aniso}$; from our frozen solution studies we can extract $(A_x + A_y + A_z)/3 = A_{iso} = A_C + A_{PC}$. For the $S = 1$ Fe^{IV}=O complexes reported so far, $\mathbf{A}_L$ was found to be vanishingly small, and we will assume that this holds for Fe_O as well.

As pointed out above, the parameters of Fe_O match within the uncertainties those of the mononuclear Fe^{IV}=O complex formed with the same ligand, $[LFe^{IV}(O)(NCMe)]^{2+}$. In the Mössbauer analysis section, we evaluated our data in the coordinate system $\{x, y, z\}$, the principal axis frame of the **D**-tensor of eq 2, and found that its z-axis coincided with the common symmetry axis of the EFG- and **A**-tensor of Fe_O (Table 1). Three experimental observations allow us to locate $\{x, y, z\}$ in the molecular frame of **2**. First, the z-axis coincides with the principal axes of the EFG and $\mathbf{A}_{SD}$ of Fe_O that are associated with the largest of the positive eigenvalues of these tensors. The DFT calculations with both methods indicate that the latter axes are collinear with the Fe^{IV}=O bond,[31] in agreement with our previous studies of Fe^{IV}=O complexes.[32,33] Second, from our Mössbauer analysis we deduced for Fe_{OH} that the largest component of the (≈axial) EFG and the smallest component of the (rhombic) **A**-tensor of Fe_{OH} (corresponding to the largest component of $\mathbf{A}_{SD}$) are essentially directed along x, a conclusion supported by the DFT calculation with method 1 which places these components at an angle of only ∼18° relative to the N−N direction of the *trans* nitrogens. Third, it follows that the y-direction, the easy axis of magnetization (see Figure 4), is then nearly along the Fe_O-O_B bond (see Figure 5). For our Mössbauer data analysis we made the assumption that the EFG- and **A**-tensors of both sites are collinear. Given that the Fe−O−Fe angle of the linking oxo bridge is 131°, rather than 90° or 180°, one would suspect that this assumption might not be correct. However, our assumption finds some support from the DFT calculations with method 1: the principal axes

(30) The Debye−Waller factor is given by the expression $f = \exp\{-E_\gamma^2\langle x^2\rangle/(\hbar c)^2)\}$ where $E_\gamma = 14.37$ KeV and $\langle x^2\rangle$ is the mean square vibrational amplitude along direction x.

(31) We will refer to "collinear" axes when the angles between them are less than 10°.

(32) Chanda, A.; Shan, X.; Chakrabarti, M.; Ellis, W. C.; Popescu, D. L.; Tiago de Oliveira, F.; Wang, D.; Que, L., Jr.; Collins, T. J.; Münck, E.; Bominaar, E. L. *Inorg. Chem.* **2008**, *47*, 3669–3678.

(33) Sinnecker, S.; Slep, L. D.; Bill, E.; Neese, F. *Inorg. Chem.* **2005**, *44*, 2245–2254.

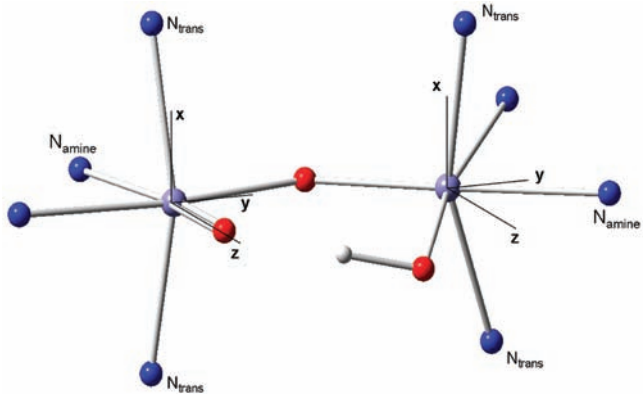

Figure 5. Direction of the axes of $\{x, y, z\}$ in the molecular structure of **2**, according to DFT calculations. z is nearly parallel to the Fe−O bond of Fe_O (left), y is within 5° parallel to Fe_O−O_B, and x is roughly parallel to the *trans* N−N direction.

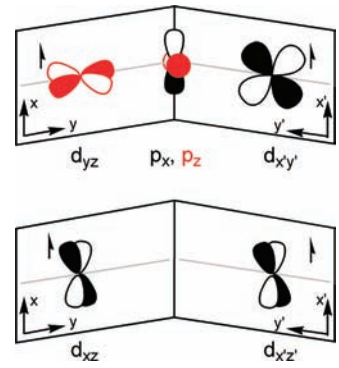

Figure 6. Magnetically active orbitals on Fe_O (left) and Fe_{OH}. The p_x and p_z orbitals reside on the bridging oxo group, O_B. Coordinate system $\{x, y, z\}$ coincides with the main reference frame in the text. $\{x',y',z'\}$ is a local frame at Fe_{OH}; x and x' are parallel.

associated with the EFG components (2.15, −1.36, −0.79) mm/s at Fe_{OH} deviate by 17°, 11°, 19° from the x, y, z axes, respectively; the $\mathbf{A}_{SD}$ components (14.2, −11.0, −3.2) T are off by 18°, 25°, 20° (for Fe_{OH} the Mössbauer analysis cannot fix the tensor axes to better than ≈20° and is thus consistent with the results of method 1). Thus, the principal axes of the **A**- and EFG-tensors are roughly aligned with the axes of **D**,[31] and neither the EFG- nor the **A**-tensor of Fe_{OH} has a principal axis coinciding with the Fe_{OH}−O_B or Fe_{OH}−O_H bond. The calculations with method 2 give much larger deviations, which is one of the reasons (see above) for focusing in the discussion on the results obtained with method 1.

The ^{57}Fe **A**-tensor of Fe_O has $A_{iso} = -16.9$ T, in excellent agreement with $A_{iso} = -16.7$ T obtained for the mononuclear site of $[LFe^{IV}(O)(NCMe)]^{2+}$. The spin-dipolar term, $\mathbf{A}_{SD} = \mathbf{A} - A_{iso}$, of Fe_O, $\mathbf{A}_{SD;x,y,z}/g_n\beta_n = (-6.1, -5.8, +11.9)$ T, is quite well represented by DFT, (−4.0, −5.9, +9.8) T; see Table S2. While the experimental data suggest a nearly axial EFG ($\eta \approx 0$) for Fe_O, method 1 gives a rhombic tensor ($\eta \approx 1.28$; in proper frame: $\eta \approx 0.75$) and a quadrupole splitting, $\Delta E_Q(\text{DFT}) = -0.80$ mm/s, with reversed sign relative to experiment, $\Delta E_Q = +0.92$ mm/s. However, the negative component (−0.80 mm/s) is aligned along y, and the calculated EFG has a positive component of 0.64 mm/s along x, in good agreement with the experimental value of 0.92 mm/s. Method 2 gives for Fe_O a less rhombic EFG ($\eta \approx 0.50$) with a positive quadrupole splitting, $\Delta E_Q = +1.57$ mm/s, along z. We have frequently observed that our DFT calculations with method 2 yield ΔE_Q values that differ by approximately 0.5−0.7 mm/s from the experimental data, and we are thus not surprised by the present discrepancy. However, for the $[LFe^{IV}(O)(NCMe)]^{2+}$ complex, the calculated and experimental ΔE_Q and η values obtained with method 2 agree, perhaps somewhat fortuitously, within 0.02 mm/s and 0.02, respectively; the calculated and experimental isomer shift agree quite nicely within 0.05 mm/s. As observed for other Fe^{IV}=O complexes obtained with TPA or TPA-related ligands, the calculated isomer shifts for Fe_O and $[LFe^{IV}(O)(NCMe)]^{2+}$ with method 2 both are 0.06 mm/s larger than the experimental values, but nevertheless in good agreement with the data. (Isomer shifts have been evaluated here with method 2, for which a calibration is available.) The reader may wonder why there is such a good agreement between the Mössbauer parameters of the Fe^{IV} sites of Fe_O and $[LFe^{IV}(O)(NCMe)]^{2+}$, given that the MeCN ligand of the latter complex is replaced by O_B in Fe_O. We have observed previously that a ligand substitution *cis* to the oxo group has little effect on the Mössbauer parameters.[34] The difference in the η values predicted for Fe_O with methods 1 and 2 may arise from the difference in the Fe_O−O_B distances with the two methods: 1.891 Å (1) and 1.993 Å (2) (see Supporting Information).

The Fe_{OH} site of **2** has a remarkably small A_{iso} value, namely $A_{iso}/g_n\beta_n = -10.2$ T, which can be compared with $A_{iso}/g_n\beta_n$ values for nonoxo complexes $[(\beta\text{-BPMCN})Fe^{IV}(OH)(OO^tBu)]^{2+}$ (−14.1 T)[35] and $[(Me_3\text{-cyclam-acetate})Fe^{IV}(N_3)]^{2+}$ (−11.8 T).[36] The small A_{iso} value of Fe_{OH} may reflect an orbital contribution opposing the Fermi contact term. For example, if the **g**-tensor of Fe_{OH} had $g_{av} = (g_x + g_y + g_z)/3 \approx 2.11$, a pseudocontact $A_{PC}/g_n\beta_n = (g_{av} - 2)P \approx +5$ T would result. (If we reasonably assume that the orbital term is negligible for $[LFe^{IV}(O)(NCMe)]^{2+}$, we obtain $P = 2\beta\langle r^{-3}\rangle \approx +45$ T for that complex.) Deviation of g-values from $g = 2.0$ is the result of spin−orbit coupling of the (local) $S_b = 1$ multiplet with excited $S_b = 1$ multiplets, and typically only one or two components of **g** are affected. Thus, a $g_{iso} = 2.11$ would suggest an anisotropic **g**-tensor, resulting in a substantial $\mathbf{A}_{L,aniso}$ contribution to the **A**-tensor of Fe_{OH}. We presently do not have sufficient information to analyze the experimental **A**-values of Fe_{OH} in more detail. The ΔE_Q of Fe_{OH} calculated with method 1 comes out about right (+2.15 mm/s vs +1.96 mm/s experimental).

Using the Mulliken gross orbital populations for the ferromagnetic state of **2** as a guideline (Tables S3 and S4), we have identified the 3d configuration of Fe_O as $(d_{xy})^2(d_{xz})^1(d_{yz})^1$ and the configuration of Fe_{OH} as an idealized $(d'_{y'z'})^2(d'_{x'y'})^1(d'_{x'z'})^1$ configuration; with $x' \parallel N_{trans}$−N_{trans}, $y' \parallel Fe_{OH}$−O_B, and $z' \parallel Fe_{OH}$−O_H, see Figure 6. Accordingly, the spin density profiles of the irons in Figure S11 exhibit cylindrical symmetry along the orthogonal z and $x' \approx x$ axes, respectively. The electronic structure of the Fe_O site is very similar to those of the well studied mononuclear $S = 1$, Fe^{IV}=O complexes,[32−34,37] resulting in hyperfine parameters for Fe_O that are similar to those found for the mononuclear $[LFe^{IV}(O)(NCMe)]^{2+}$ complex. The valence contributions to the EFGs obtained for the two configurations

(34) Rohde, J. U.; Stubna, A.; Bominaar, E. L.; Münck, E.; Nam, W.; Que, L. *Inorg. Chem.* **2006**, *45*, 6435–6445.
(35) A_{za} comes only into play for applied fields $B \geq 6$ T. It is possible to increase A_{za} from −20 to −26 T without serious deterioration of the simulation, and thus an $A_{iso}/g_n\beta_n = -12.2$ T is possible for site **a**.
(36) Berry, J. F.; Bill, E.; Bothe, E.; Weyhermüller, T.; Wieghardt, K. *J. Am. Chem. Soc.* **2005**, *127*, 11550–11551.
(37) Decker, A.; Solomon, E. I. *Angew. Chem., Int. Ed.* **2005**, *44*, 2252–2255.

generate axial tensors with large, positive components along z (at Fe_O) and along x' (at Fe_{OH}, x' is nearly parallel to x), consistent with the perpendicular orientation deduced from the Mössbauer analysis. As expected for these configurations, the spin−dipolar contributions to the **A**-tensor from method 1, $\mathbf{A}_{SD}$ = (−4.0, −5.9, +9.8) T for Fe_O and $\mathbf{A}_{SD}$ = (+14.2, −11.0, −3.2) T for Fe_{OH}, have large positive components along z and $x' \approx x$, respectively, but with a significant degree of rhombicity in the yz plane at Fe_{OH}, indicating that the $(d'_{y'z'})^2(d'_{x'y'})^1(d'_{x'z'})^1$ configuration must be considered as an idealization of the DFT solution. As shown in Figure S11, the p_x orbitals at both the bridging and hydroxo oxygen atoms carry significant spin densities, indicating the presence of sizable π interactions of these orbitals with the $d'_{x'y'}$ and $d'_{x'z'}$ orbitals of Fe_{OH}, respectively, pushing the latter up in energy and leaving the $d'_{y'z'}$ orbital as the lowest, doubly occupied t_{2g} orbital. The π interactions with pyridines, which are good σ donors, play probably a lesser role in removing the degeneracy of the t_{2g} orbitals. Spin−orbit coupling of the ground-state with the spin-allowed excitations $d'_{y'z'} \rightarrow d'_{x'z'}$ and $d'_{y'z'} \rightarrow d'_{x'y'}$ yield unquenched orbital moments along z' and y'. The associated magnetic moments give a (positive) pseudocontact term which may explain the low value for A_{iso} deduced from the spin-Hamiltonian analysis. In particular, these contributions allow us to adopt a more realistic Fermi contact term. For example, by combining $A_C = -14$ T, the value for $[(\beta\text{-BPMCN})Fe^{IV}(OH)(OOtBu)]^{2+}$, with $\mathbf{A}_{SD}$ = (+14.2, −11.0, −3.2) T from DFT and an A_L = (+0.2, +14.0, −2.8) T we obtain the $\mathbf{A}_{tot}$ = (+0.4, −11.0, −20.0) T observed. The A_L components suggest that the energies of the t_{2g} orbitals appear in the order $d'_{y'z'} < d'_{x'y'} < d'_{x'z'}$. The zero-field splitting tensor is axial along x' when the t_{2g} excitations are degenerate and rhombic ($0 < E/D \leq {}^1/_3$) when they are nondegenerate. The latter situation is likely to apply, given the difference in the π ligand interactions of the two excited t_{2g} orbitals. This analysis suggests that the zero-field splitting at Fe_{OH} results from spin−orbit coupling of the ground-state with excited-states of the same local spin ($S_{loc} = 1$) and not from spin−orbit coupling with a low-lying $S_{loc} = 2$ excited-state as is likely the case at the Fe_O site.[32]

Why is Complex 2 Ferromagnetic?

Finally, we wish to address why complex **2** is ferromagnetic. Our broken-symmetry calculations, using method 1, predict an exchange-coupling constant $J = -320$ cm^{-1} for **2**. This value is surprisingly large and exceeds, perhaps, the magnitude of the optimal J value deduced from the Mössbauer analysis. There is an extensive literature about the relationship between exchange interactions and molecular structure.[38−43] In these theoretical contributions, J is expressed as the sum of a ferromagnetic and an antiferromagnetic term, $J = J_F + J_{AF}$ ($J_F < 0$, $J_{AF} > 0$). The magnitudes of J_F and J_{AF} are determined by the overlap properties of unpaired-electron-containing ("magnetic") orbitals at the interacting metal centers that are defined by their respective ligand environments.[44,45] In the case that the magnetic orbitals are nonorthogonal, J_{AF} is nonzero and often the dominant term, resulting in a net antiferromangetic exchange interaction, $J > 0$.

The orbitals containing the unpaired electrons are illustrated in Figure 6: d_{yz} and d_{xz} at Fe_O and $d'_{x'y'}$ and $d'_{x'z'}$ at Fe_{OH}. For reasons of orbital symmetry, the orbitals d_{xz} and $d'_{x'z'}$ are unfavorable for mixing with the orbitals of the bridging oxygen and contribute little to J due to vanishing overlap density between them. The orbitals d_{yz} at Fe_O and $d'_{x'y'}$ at Fe_{OH} match the p_z and p_x orbitals of the bridging oxygen in symmetry, leading to the formation of magnetic orbitals with composition $d_\pi \approx d_{yz} + c_z p_z$ and $d'_{\pi'} \approx d'_{x'y'} + c_{x'} p_x$, where $c_{x'}$ and c_z are small mixing coefficients. (The spin densities suggest that $|c_z| \ll |c_{x'}|$, cf., Supporting Information.) The magnetic orbitals d_π and $d'_{\pi'}$ have nonvanishing overlap density at the bridging oxygen because the product function $c_x c_z p_x(r) p_z(r)$ is not identical to zero. The associated overlap integral, however, is zero: $\langle d_\pi | d'_{\pi'} \rangle \approx c_z c_x \langle p_z | p_x \rangle = c_z c_x \int p_z(r) p_x(r) dr^3 = 0$. Since the orbitals d_π and $d'_{\pi'}$ have a nonvanishing overlap density for which the spatial integral is zero, the condition for ferromagnetic exchange between the unpaired electrons in these orbitals and thus for ferromagnetic exchange coupling between the spins $S_a = S_b = 1$ of Fe_O and Fe_{OH} is fulfilled. If this interpretation of the DFT results for J is valid, then we have identified a system where the inequivalent coordination of the paramagnetic sites is instrumental in defining the magnetic orbitals in a way favorable for ferromagnetic exchange.

In closing, we wish to stress that, due to lack of experimental data, we have no experience in assessing the quality of calculated J-values for diiron(IV) complexes by DFT methods. For the system at hand, we alert the reader that if the core unit of **2** is nonplanar, as suggested by DFT method 2 (see Supporting Information), the magnetic orbitals may have nonorthogonal pathways, leading to antiferromagnetic contributions to the exchange-coupling constant and thus to smaller J values. The analysis of Mössbauer spectra of **2** is exceedingly complex as it may entail as many as 38 unknowns (for C_1 symmetry), not counting uncertainties introduced by removing contributions of contaminants. At this time we have to be content with noting that both theory and experiment indicate substantial ferromagnetic coupling for this interesting diron(IV) complex.

Acknowledgment. This work was supported by NIH Grants GM38767 (to L.Q.) and EB0001474 (to E.M.), by NSF grants MCB-0424494 (to E.M.) and CHE070073 (to E.L.B.) through TeraGrid resources provided by the NCSA, and by an NIH postdoctoral fellowship GM-079839 to A.T.F.

Supporting Information Available: Mössbauer and DFT analysis for $[LFe^{IV}(O)(NCMe)]^{2+}$ and details on the methods and results for the DFT study of **2**. This material is available free of charge via the Internet at http://pubs.acs.org.

JA8098917

(38) Goodenough, J. B. *Phys. Rev.* **1955**, *100*, 564–573.
(39) Kanamori, J. *J. Phys. Chem. Solids* **1959**, *10*, 87–98.
(40) Anderson, P. W. *Phys. Rev.* **1959**, *115*, 2–13.
(41) Goodenough, J. B. *Magnetism and the Chemical Bond*; Wiley and Sons: New York, 1963.
(42) Anderson, P. W. In *Magnetism*; Academic Press: New York, 1963; Vol. 1, p 25.
(43) Hotzelmann, R.; Wieghardt, K.; Florke, U.; Haupt, H. J.; Weatherburn, D. C.; Bonvoisin, J.; Blondin, G.; Girerd, J. J. *J. Am. Chem. Soc.* **1992**, *114*, 1681–1696.
(44) Kahn, O.; Briat, B. *J. Chem. Soc., Faraday Trans. 2* **1976**, *72*, 268–281.
(45) Bominaar, E. L.; Block, R. *Physica B & C* **1983**, *121*, 109–120.